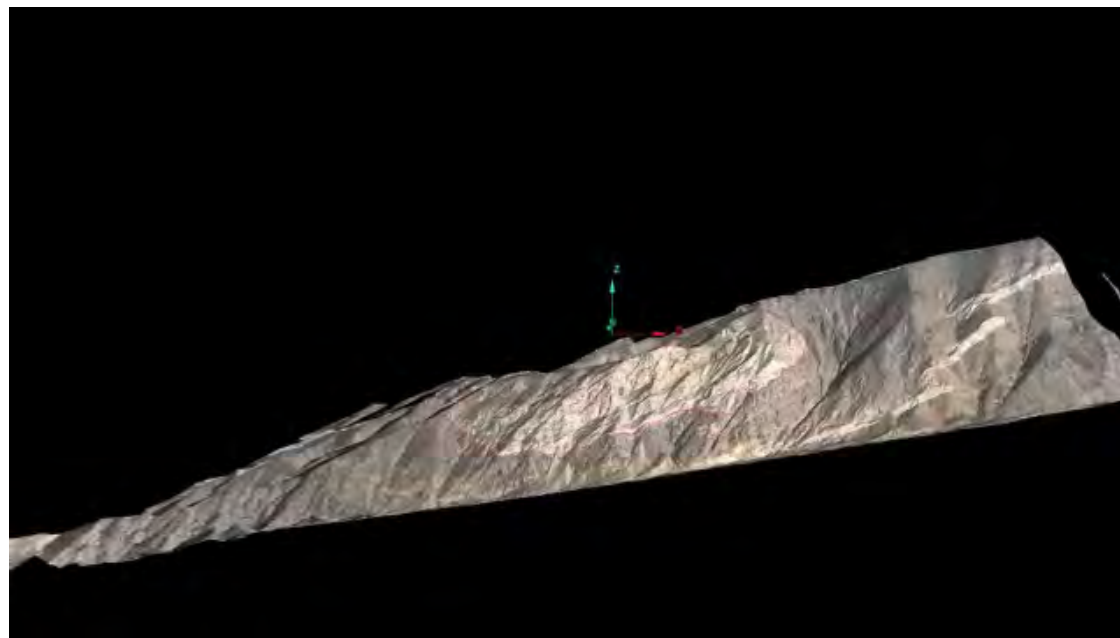section with the point cloud or TIN model surface. I-Site Studio can also use multiple points or triangular patches in the TIN to calculate a best-fit orientation, a method referred to as "patch selection". These routines provide the ability to extract orientation data for cliff faces and other areas inaccessible in the field. However, they require an accurate terrain model and the ability for a user to visualize the surface and evaluate the validity of the geologic interpretation without the benefit of ground-truth measurements (Animation 2).

To evaluate the application of these remote orientation measurement techniques, we analyzed two sites in Pleasant Canyon: Clair Camp and Noonday. For the Clair Camp site (Figs. 10A and 10B), orientations obtained from the TLS terrain model could be directly compared to field measurements, whereas most of the Noonday site (Figs. 10C and 10D) is an inaccessible cliff face (Animation 2). Thus, for the Noonday structure we can only compare the MVS model–derived orientations to field measurements from outcrops at the base of the cliff, from the ridge tops, and from the south side of the canyon. In all cases, the orientation analysis was done either with a simple three- to six-point analysis from the point cloud or using patch selection on a slope that was interpreted to show exposed layering on the terrain model. The TLS model was used at the Clair Camp site because of the inaccuracy of the MVS model (see above), but the results would undoubtedly be similar from a more closely aligned MVS model. At the Noonday site, we chose to use the MVS model to extract orientations because it had been aligned to the TLS model.

A stereographic plot of 30 TLS-derived strike-and-dip orientations of S1 foliation from the Clair Camp site is similar to that of the 30 orientations taken in the field (Figs. 10A and 10B). Both stereograms show: (1) dominantly west-dipping foliation with dips that range from shallow to steep as a result of younger folding of foliation; and (2) a π-pole in the southwest quadrant reflecting the axis of the fold in foliation that is easily seen on the hillslope (Fig. 3A, at north end of the easternmost purple zone [quartzite] there is a fold in foliation [black lines] and the axial trace of that fold is indicated by a blue line). The π-pole for the TLS-derived orientations plunges 35° toward azimuth 215°, whereas the π-pole from the field orientations plunges 18° toward 193°. The scatter, however, is different between the two stereograms. The TLS-derived measurements display a greater angular dispersion around the fold than the field measurements, providing a clearer definition of the fold orientation for this structure. The field data have greater azimuthal scatter over a more constant dip range, primarily reflecting small-scale variations that are not visible on the model. Nonetheless, the results are comparable and reasonably acceptable. The similarity in results between the two techniques in this area probably reflects the relative ease of recognizing foliation surfaces in the TLS model in an area dominated by relatively flaggy schists.

The measurements of foliation at the Noonday structure (Figs. 10C and 10D) are more difficult to interpret. The field data (Fig. 10D) display a classic great-circle distribution of foliation poles with a well-defined π-pole that

If reading the full-text version of this paper, please download article PDF to view Animation 2 in Adobe Acrobat or Adobe Reader. It is also available by visiting http://doi.org/10.1130/GES01691.a2 or the full-text article on www.gsapubs.org.

Animation 2. Visualization of the multi-view stereo–derived triangulated irregular network of the Noonday structure. The pink line represents the basal contact of the Noonday Dolomite (light-colored rock that caps the ridge) and is an example of direct mapping on a three-dimensional model (see text for discussion). Refer to Figure 3B for scale. This video was made using I-Site Studio software. If reading the full-text version of this paper, please download article PDF to view Animation 2 in Adobe Acrobat or Adobe Reader. It is also available by visiting http://doi.org/10.1130/GES01691.a2 or the full-text article on www.gsapubs.org.